International Journal of Applied Earth Observation and Geoinformation 18 (2012) 491–503

Contents lists available at SciVerse ScienceDirect

International Journal of Applied Earth Observation and Geoinformation

journal homepage: www.elsevier.com/locate/jag

Collinearity and orthogonality of endmembers in linear spectral unmixing

Freek D. Van der Meer[a,*], Xiuping Jia[b,1]

[a] University of Twente, Faculty of Geo-information Science and Earth Observation (ITC), Hengelosestraat 99, 7514 AE Enschede, The Netherlands
[b] School of Engineering and Information Technology, University College, The University of New South Wales, Campbell, ACT 2600, Australia

ARTICLE INFO

Article history:
Received 10 February 2011
Accepted 6 October 2011

Keywords:
Collinearity
Orthogonality
Endmembers
Linear spectral unmixing

ABSTRACT

Contrary to image classification, spectral unmixing techniques allow to derive abundance/fractional cover estimates for selected endmembers within the volume of a pixel. Mathematically the solution to the mixing problem is resolving a set of linear equations using least squares approaches. Practically this is done using singular value deconvolution of the endmember matrix inversion. This solution assumes orthogonality of the endmembers which determines the orthogonality of the matrix. If endmembers are highly correlated (thus collinearity or multi-collinearity occurs), the matrix becomes non-orthogonal, the inversion unstable and the inverse or estimated fractions highly sensitive to random error (e.g., noise). In practice, collinearity almost always exists but it is typically overlooked or ignored, hence with this overview we wish to create awareness to the issue and offer approaches to deal with the problem. The first part of the paper highlights the problem using a numerical example. It is shown how collinearity amplifies the error in the endmember matrix inversion. In the next paragraph we propose measures to quantify the level of (multi)collinearity in the endmember matrix: a weighted multiple correlation measure, the variance inflation factor, the partial regression coefficient. The remainder of the paper is dedicated to approaches to mitigate the problem: excluding endmembers, decorrelating endmembers, iterative approaches for endmember selection and we propose an adjustment to the unmixing equation which could be further explored. In conclusion, collinearity hampers the use of fractional abundance estimates. There is no single recipe to successfully combat this problem but in all mixture models collinearity should be tested and avoided as much as possible.

1. Introduction

Traditional image classification aims at representing the landscape in terms of a number of fixed classes where each image pixel has a unique class label. On the contrary, mixture modeling and spectral unmixing (Settle and Drake, 1993) strive at representing ground cover classes within pixels as relative or absolute fractions (also referred to as abundance) of a number of (spectral) components or endmembers. While mixture modeling allows modeling a mixed spectrum based on pure endmember spectra, the outcome of spectral unmixing analysis is a new set of images that for each selected endmember portray the fraction of this class within the volume bound by the pixel. Thus mixture modeling is the forward process of deriving mixed signals from pure endmember spectra while spectral unmixing aims at doing the reverse, deriving the fractions of the pure endmembers from the mixed pixel signal. Spectral unmixing is a popular tool to arrive at fractional surface cover from multi- and hyperspectral remote sensing data sets and recent papers can be found covering a wide range of applications including land use/land cover mapping (Foody and Cox, 1994; Asner and Heidebrecht, 2002; Lu et al., 2004), erosion and land degradation studies (de Jong et al., 1999; Metternicht and Fermont, 1998), estimation of biophysical properties (Asner and Lobell, 2000; Okin et al., 2001), agricultural applications (Lelong et al., 1998), water quality studies (Hedley and Mumby, 2003), urban studies (Roessner et al., 2001; Segl et al., 2003) and mineral exploration (Kruse et al., 1993; Neville et al., 2003; Hecker et al., 2010). Despite its popularity, there are some inherent issues related to the inversion of the mixtures resulting in estimated fractions that are typically overlooked in many of these applied studies. This is the topic of our paper.

A good introductory text to spectral unmixing is found in Settle and Drake (1993) and Keshava and Mustard (2002). In general, a linear combination of spectral endmembers is chosen to decompose the mixed reflectance spectrum of each pixel r_i into fractions f_j of its endmembers r_{ji} by

$$r_i = \sum_{j=1}^{n} f_j r_{ji} + \varepsilon_i, \quad i = 1, \ldots, L \tag{1}$$

* Corresponding author. Tel.: +31 53 4874353; fax: +31 53 4874336.
E-mail addresses: vdmeer@itc.nl (F.D. Van der Meer), x.jia@adfa.edu.au (X. Jia).
[1] Tel.: +61 2 626 88202; fax +61 2 626 88443.

1569-8432/$ – see front matter © 2011 Elsevier B.V. All rights reserved.
doi:10.1016/j.jag.2011.10.004

where r_i is the reflectance of the mixed spectrum in image band i (of L) for each pixel, f_j is the fraction of each endmember j calculated band by band, r_{ji} is the reflectance of the endmember spectrum j in band i, i is the band number, j is each of the n image endmembers and ε_i is the residual error (unexplained variance which typically contains noise). An additional constraint can be that the fractions sum to 1 and are non-negative for each endmember. A unique solution is found from Eq. (1) by minimizing the residual error ε_i through a least-squares solution. Eq. (1) can be solved through a singular value decomposition (SVD) matrix inversion (which we adopt in this paper) although several other methods (e.g., sequential quadratic programming (Chen et al., 2009), Gaussian mixture discriminant analysis (Ju et al., 2003), subspace projection techniques (Harsanyi and Chang, 1994; Chang et al., 1998)) have been implemented. SVD works well with orthogonal endmembers (perpendicular spectral vectors), but with increasing non-orthogonality the matrix tends to become singular (i.e., the matrix is ill-conditioned and the determinant is near to 0) and unstable or (worse) cannot be inverted (Van der Meer and De Jong, 2000a). If all endmembers are spectrally unique, all singular values are equal, however for a degenerate set of endmembers all but one singular value will be zero. Non-orthogonality of endmember spectra is the case when collinearity (two input endmember spectra are highly correlated) or multicollinearity (several input endmember spectra are highly correlated) exists (Graham, 2003). In this case the mixing model tends to become unstable, which is expressed in a large error term, a mixing model that is sensitive to small changes in input spectra and highly sensitive to noise. The latter is shown by model simulation conducted in (Chen et al., 2010). It should be noted that also cross correlation exists within (particular hyperspectral) endmember spectra as band-to-band correlation leads to data redundancy which in turn contributes to intrinsic-spectral collinearity.

Spectral unmixing has become a popular technique with the advent of hyperspectral sensors, however is also frequently used to analyze multispectral images. Hyperspectral sensors carry many (hundreds), contiguous (partly redundant, e.g., due to overlapping spectral response functions capturing similar spectral surface radiance characteristics) spectral bands. In most spectral unmixing studies, the residual error (not the ε_i!) or the difference between the measured and modeled mixed pixel spectrum is calculated as a root-mean square (RMS) error. The RMS is the difference of the measured $r_i^{(k)}$ and modeled pixel spectrum $r_i^{(k)'}$ as

$$\mathrm{rms} = \sqrt{\frac{\sum_{k=1}^{m}\sum_{i=1}^{L}\left(r_i^{(k)} - r_i^{(k)'}\right)^2}{mL}} = \sqrt{\frac{\sum_{k=1}^{m}\sum_{i=1}^{L}\left(\varepsilon_i^{(k)}\right)^2}{mL}} \qquad (2)$$

for L spectral bands and m pixels.

The issue of (multi- and intra) collinearity is grossly overlooked although it seriously affects the mixture model and hampers the reliability and usefulness of fraction/abundance estimates. In this paper we revisit the collinearity problem by taking a numerical look at spectral inversions through spectral unmixing. Next we explore ways to 'measure collinearity' and we discuss ways to 'reduce the effect of collinearity' hoping to create awareness of this problem particularly under the readily growing user community of unmixing techniques.

2. The collinearity problem revisited

2.1. An historical perspective

Spectroscopy is the study of light as a function of wavelength emitted, reflected or scattered from a medium with the aim of relating absorpted and reflected radiation to physical and chemical properties of substances. In the 1970s, a group led by Graham Hunt and John Salisbury studied reflectance spectra of minerals and rocks and published a series of articles in a journal called *Modern Geology* which formed the basis of modern spectral libraries (Hunt, 1977). Early work on Martian geology soon later started a discussion on spectra of mixtures and mixed signals observed in Lunar images (Singer and McCord, 1979), which in turn led to fundamental work on linear and nonlinear behavior of light in mineral grains (Clark, 1983; Singer, 1981). Papers published on this topic in the early 1980s primarily focused on spectral mixing (mixture modeling) of reflectance spectra to try to explain the observations in six channel Viking Lander images from Mars (Adams et al., 1986). Alongside more fundamental work based on radiative transfer using the Kubalka–Munk theory (Johnson et al., 1983) tried to give answers to binary mineral spectral mixing. With the increase in computing power by the end of the 1980s and earl 1990s the first papers appeared on spectral unmixing and estimation of fractional abundances. The work of Boardman (1989) and Settle and Drake (1993) was instrumental in developing the early inversion methods that formed the basis of spectral unmixing. Alongside the advent of high spectral resolution remote sensing in particular the NASA Jet Propulsion Laboratory operated Airborne Visible/Infrared Imaging Spectrometer (Vane et al., 1993) made possible the collection of image data in many, narrow and contiguous spectral bands and inspired many to unravel the Earth surface composition at a subpixel level. After the initial successes, several researchers started pointing out some of the inherent complexities of working with fractional abundances related to spectral confusion on the one hand and instrument deficiencies on the other hand.

Spectral mixture analysis was used to determine the threshold detection limits of target materials in the presence of background materials by simulating the effect of spectral sampling, noise and illumination conditions (Sabol et al., 1992). It was concluded that for a given imaging system detection of surface materials can be optimized by making image measurements during lighting conditions, knowing the spectra of the endmembers that contribute to the mixing, selecting a spatial scale of observation that minimizes the variability of each endmember, and selecting bands that maximize contrast of target spectra against background spectra. Another early study, showed the potential of using the residuals resulting from the inversion in spectral unmixing statistics which allowed reducing the spectral confusion between the nonphotosynthetic vegetation (NPV) and soil endmember (Roberts et al., 1993). Price (1994) addressed the question "How unique are spectral signatures?" focusing on the representativeness of spectral signatures as endmembers for unmixing. The main conclusion was that 'a spectrum from one vegetation species may correspond closely to a mixture of spectra from other species' thus the main message was that 'spectral unmixing must be approached with caution'. Also work focused on measuring changes over time using a four endmember (green vegetation, NPV, soil and shade) model and investigating the sources of classification error related to system noise, endmember variability and low spectral contrast (Adams et al., 1995). Soon several researchers started experimenting with methods by which endmembers are derived from the image data itself (Tompkins et al., 1997). In these modified spectral mixture analysis approaches, the inversion of the unmixing matrix now included both the spectral endmembers as well as the fractional abundances as unknowns. This meant that rather than a single pixel, all image pixels were modeled simultaneously and thus the size of the matrix to be solved varied with the number of bands, number of endmembers and the number of image pixels. Multiple endmember spectral mixture model that allows type and number of endmember spectra to vary per pixel were soon introduced and their theory firmly established (Roberts et al., 1998). On a per pixel

basis the RMS error and the residuals were used to optimize the model.

The sensitivity of linear unmixing to system noise was recognized in the early days of spectral unmixing (Settle and Drake, 1993). A fundamental paper to the issue of collinearity in the inversion of models in spectral unmixing was published in 1999 (Drake et al., 1999). These authors used spectral matching of pure library spectra against image pixel spectra as a way of identifying endmembers. Next they built a mixture model that allowed estimating errors on the proportion estimates. In an iterative way they discarded the endmembers which produced the highest error and recomputed the fractions until a relatively noise free mixture model was obtained. Although the results are considerably improved by dropping endmembers, the disadvantage lies in the fact that it is likely that for some end user an important surface material or property is discarded in the analysis as it may be dropped. For example, in the underlying case kaolinite was dropped from the endmember list because it produced notable errors on the proportions, however from a geologic perspective (the area studied was hydrothermally altered) kaolinite is one of the key minerals to mapping alteration. Several good review articles have been published that give a good chronological perspective on the developments of spectral unmixing and hyperspectral (imaging spectrometry/spectroscopy) remote sensing with emphasis on spectral mixture analysis (Adams et al., 1993), mixture modeling versus sub-pixel methods (Ichoku and Karnieli, 1996), analytical techniques in hyperspectral analysis (Cloutis, 1996), and endmember variability (Somers et al., 2011) and there are some textbooks on the topic (Chang, 2003; Van der Meer and De Jong, 2000b).

2.2. Inversion of the spectral unmixing system of equations

Eq. (1) is typically solved through an inversion of the matrix (Settle and Drake, 1993).

$$\boldsymbol{r} = \boldsymbol{M}f + \varepsilon \tag{3}$$

where $\boldsymbol{r}$ is the vector (i x 1) radiance/reflectance target/pixel spectrum, $\boldsymbol{M}$ is a (i x j) matrix composed of endmember spectra and ε is a (i x 1) noise vector. The fractions/abundances f (a (j x 1) vector) for each endmember are found by inverting Eq. (3) (applying no sum to 1 constraints) as

$$\hat{f} = (\boldsymbol{M}^T\boldsymbol{M})^{-1}\boldsymbol{M}^T\boldsymbol{r} \tag{4}$$

The inversion assumes independence, however when endmembers are correlated the columns of the matrix $\boldsymbol{M}$ are linearly dependent, when band-to-band correlation is high, the rows of the matrix $\boldsymbol{M}$ are linearly dependent and in both cases the matrix ($\boldsymbol{M}^T\boldsymbol{M}$) becomes close to singular (i.e., has no inverse). Near singularity means that the smallest eigenvalue becomes the dominating factor in the inversion. As its reciprocal is very large, thus if a small error is introduced it will be extremely magnified in the inversion process.

2.3. Unmixing in the absence of noise

To illustrate the above we present numerical solutions to three cases (Case 1: low correlation between endmembers, Case 2: high correlation between two endmembers, and Case 3: high correlation between all endmembers), where we show the matrix $\boldsymbol{M}$ of 6 vectors each column representing an endmember spectrum, its inverse $(\boldsymbol{M}^T\boldsymbol{M})^{-1}$ and the resulting numerical solution to unmix mixed vector (Settle and Drake, 1993; Foody and Cox, 1994; Segl et al., 2003; Chen et al., 2010; Price, 1994; Nascimento and Dias, 2005). The unmixing model we used applies no constraints such as 'sum to one' and 'positive fractions' and thus is fully unconstrained. Case 2 can be considered the collinear case while Case 3 is the multicollinear case.

2.3.1. Case 1 (low correlation between endmembers)

In this case the endmember matrix used is:

$$\boldsymbol{M} = \begin{bmatrix} 10 & 222 & 23 & 33 & 50 & 12 \\ 100 & 250 & 26 & 34 & 120 & 60 \\ 140 & 234 & 24 & 34 & 60 & 80 \\ 160 & 223 & 25 & 232 & 150 & 50 \\ 100 & 212 & 23 & 112 & 150 & 150 \\ 80 & 211 & 25 & 100 & 150 & 22 \end{bmatrix} \tag{5}$$

The associated correlation matrix ρ shows a moderate (max 0.692 between endmembers 4 and 5) cross correlation between the spectra

$$\rho = \begin{bmatrix} 1 & 0.206 & 0.420 & 0.551 & 0.411 & 0.408 \\ 0.206 & 1 & 0.553 & 0.206 & -0.344 & -0.081 \\ 0.420 & 0.553 & 1 & 0.420 & 0.400 & -0.315 \\ 0.551 & -0.426 & 0.155 & 1 & 0.692 & 0.092 \\ 0.411 & -0.344 & 0.400 & 0.692 & 1 & 0.302 \\ 0.408 & -0.081 & -0.315 & 0.092 & 0.302 & 1 \end{bmatrix} \tag{6}$$

The inverse endmember matrix $(\boldsymbol{M}^T\boldsymbol{M})^{-1}$ is

$$(\boldsymbol{M}^T\boldsymbol{M})^{-1} = \begin{bmatrix} -0.0081 & 0.0025 & 0.0068 & 0.0016 & -0.0047 & 0.0010 \\ 0.0053 & 0.0547 & -0.0298 & 0.0182 & -0.0057 & -0.0461 \\ 0.0033 & -0.5604 & 0.3154 & -0.1855 & 0.0506 & 0.4560 \\ 0.0042 & -0.0046 & -0.0023 & 0.0057 & 0.0014 & -0.0039 \\ -0.0067 & 0.0194 & -0.0132 & 0.0011 & -0.0002 & -0.0022 \\ 0.0008 & -0.0091 & 0.0043 & -0.0038 & 0.0092 & -0.0001 \end{bmatrix} \tag{7}$$

2.3.2. Case 2 (high correlation between two endmembers, e.g., the collinear case)

Now we replaced endmember 6 by an endmember that is nearly identical to endmember 5 as

$$\boldsymbol{M} = \begin{bmatrix} 10 & 222 & 23 & 33 & 12 & 12 \\ 100 & 250 & 26 & 34 & 60 & 60 \\ 140 & 234 & 24 & 34 & 80 & 80 \\ 160 & 223 & 25 & 232 & 50 & 50 \\ 100 & 212 & 23 & 112 & 150 & 150 \\ 80 & 211 & 25 & 100 & 23 & 22 \end{bmatrix} \tag{8}$$

This is clearly shown in a high correlation of >0.999 between endmembers 5 and 6, however the average absolute correlation between the endmembers is 0.45

$$\rho = \begin{bmatrix} 1 & 0.206 & 0.420 & 0.551 & 0.408 & 0.408 \\ 0.206 & 1 & 0.553 & 0.206 & -0.085 & -0.081 \\ 0.420 & 0.553 & 1 & 0.420 & -0.313 & -0.315 \\ 0.551 & -0.426 & 0.155 & 1 & 0.093 & 0.092 \\ 0.408 & -0.085 & -0.313 & 0.093 & 1 & 0.999 \\ 0.408 & -0.081 & -0.315 & 0.092 & 0.999 & 1 \end{bmatrix} \tag{9}$$

The inverse now becomes

$$(\boldsymbol{M}^T\boldsymbol{M})^{-1} = \begin{bmatrix} -0.011 & 0.0114 & 0.007 & 0.0021 & -0.0048 & 0.0000 \\ 0.1434 & -0.3452 & 0.2427 & -0.0047 & -0.0012 & -1.6\times10^{-16} \\ -1.3602 & 3.3890 & -2.3760 & 0.0418 & 0.0064 & 1.58\times10^{-15} \\ 0.0161 & -0.0389 & 0.0211 & 0.0037 & 0.0017 & -1.8\times10^{-17} \\ 2.9901 & -8.6611 & 5.9023 & -0.4988 & 0.0969 & 1.0000 \\ -2.9889 & 8.6509 & -5.8974 & 0.4949 & -0.0876 & -1.0000 \end{bmatrix} \quad (10)$$

2.3.3. Case 3: high correlation between all endmembers (e.g., the multicollinear case)

This is an extreme case where nearly all endmembers are identical

$$\boldsymbol{M} = \begin{bmatrix} 12 & 30 & 10 & 12 & 12 & 12 \\ 60 & 65 & 60 & 60 & 60 & 60 \\ 80 & 85 & 90 & 80 & 80 & 80 \\ 50 & 51 & 50 & 55 & 50 & 50 \\ 150 & 132 & 170 & 171 & 150 & 150 \\ 21 & 30 & 10 & 21 & 23 & 22 \end{bmatrix} \quad (11)$$

The correlation matrix now becomes

$$\rho = \begin{bmatrix} 1 & 0.994 & 0.997 & 0.997 & 0.999 & 0.999 \\ 0.994 & 1 & 0.997 & 0.994 & 0.993 & 0.993 \\ 0.997 & 0.997 & 1 & 0.997 & 0.996 & 0.997 \\ 0.997 & 0.986 & 0.994 & 1 & 0.997 & 0.997 \\ 0.999 & 0.993 & 0.996 & 0.997 & 1 & 0.999 \\ 0.999 & 0.993 & 0.997 & 0.997 & 0.999 & 1 \end{bmatrix} \quad (12)$$

The inverse now becomes

$$(\boldsymbol{M}^T\boldsymbol{M})^{-1} = \begin{bmatrix} -1.78\times10^{15} & -7.03\times10^{15} & 3.93\times10^{15} & 9.00\times10^{15} & -2.14\times10^{15} & -0.5 \\ 0.0577 & -0.0676 & 0.0434 & 0.0359 & 8.89\times10^{-05} & 0 \\ 0 & -0.3428 & 0.2571 & 0.1714 & 0 & 0 \\ 0.0729 & -0.0486 & -0.0486 & 0.0486 & 0.0486 & 0 \\ -1.78\times10^{15} & -7.03\times10^{15} & 3.93\times10^{15} & 9.00\times10^{15} & -2.14\times10^{15} & 0.5 \\ 3.56\times10^{15} & 1.40\times10^{16} & -7.86\times10^{15} & -1.80\times15^{16} & 4.28\times10^{15} & 0 \end{bmatrix} \quad (13)$$

2.3.4. Unmixing results for the three cases

The results of unmixing the mixed spectrum (Settle and Drake, 1993; Foody and Cox, 1994; Segl et al., 2003; Chen et al., 2010; Price, 1994; Nascimento and Dias, 2005) with the endmember sets of Cases 1, 2, and 3 are summarized in Table 1. One can see that with an increasing correlation between the endmembers and thus an increase in non-orthogonality the matrix becomes closer to singularity as expressed in a determinant for the endmember matrix in Case 3 becoming close to zero. Although the overall absolute correlation (e.g., negative correlations negated to positive ones) of Case 1 compared to Case 2 is similar, the fact that two endmembers are highly correlated has serious consequences for the estimated fractions (resulting from numerical instability of the inversion) however this is hardly reflected in the RMS error. In the extreme Case 3, the numerical solution is highly unstable and the fractions as well as the RMS error clearly reflect this. A singular matrix (i.e., a matrix that has no inverse) has a determinant of zero which occurs when one row (or column) is filled with zeros or if two rows (or two columns) are equal or proportional to each other.

2.4. Unmixing in the presence of noise

Mixed spectra were generated with given fractions for the three cases to illustrate the unmixing performance in the presence of noise. The true fractions were set to 1/6 for each endmember (equal fraction), i.e., $f = \left[(1/6)(1/6)(1/6)(1/6)(1/6)(1/6)\right]^T$. The noise free mixed spectral vectors, $\boldsymbol{r}_a^{(q)}$, were generated by $\boldsymbol{M}_q f$, $q = 1, \ldots, 3$. The resulting spectra are the ideal ones without noise. Two mixed spectra with two introduced noise levels for each case, $\boldsymbol{r}_b^{(q)}$, and, $\boldsymbol{r}_c^{(q)}$, were generated as well. Their band 1 values were degenerated by adding a noise component to 95% and 90%, respectively, i.e.,

$$\begin{aligned} &\boldsymbol{r}_b^{(q)}(1) = 0.95\times\boldsymbol{r}_a^{(q)}(1), \text{ and } \boldsymbol{r}_b^{(q)}(i) = \boldsymbol{r}_a^{(q)}(i), \quad i = 2,\ldots,L, \quad q = 1,\ldots,3 \\ &\boldsymbol{r}_c^{(q)}(1) = 0.90\times\boldsymbol{r}_a^{(q)}(1), \text{ and } \boldsymbol{r}_c^{(q)}(i) = \boldsymbol{r}_a^{(q)}(i), \quad i = 2,\ldots,L, \quad q = 1,\ldots,3 \end{aligned} \quad (14)$$

The results of the unmixing including noise are summarized in Table 2. One can see that Case 1 works perfectly for the noise free data, and performs acceptably when noise presents. When two endmembers are highly correlated (Case 2), it becomes very sensitive to noise. The SSE is too high when a very low level of noise is introduced. Case 3 is close to singular, it does not work even when there is no noise.

2.5. An example from high resolution reflectance spectra

So far the cases presented are rather hypothetical examples where six endmembers are used to unmixing a six channel/band image data set. This mimics the case of spectral unmixing of a Landsat Thematic Mapper data set, however in most prevailing cases researchers would use 3–4 endmembers such as vegetation, soil, nonphotosynthetic vegetation and possibly an additional surface type. A more realistic example is derived from real reflectance spectra taken from the USGS mineral spectral library provided in ENVI. This library contains spectra in the 0.3951–2.56 μm region. Each spectrum consists of 420 bands with a sampling interval and band width/spectral resolution of around 0.02 μm.

From this exhaustive data set, spectra for eight minerals were selected (1, alunite; 2, buddingtonite; 3, chlorite; 4, halloysite; 5, illite; 6, kaolinite; 7, montmorillonite and 8, talc). From these a Case 1 (low correlation case), Case 2 (high correlation case) and Case 3 (multicollinear case) was generated by selecting 4 endmember spectra at the time and using a subset of 31 bands (out of the 420 bands available) as:

Case 1: Bands 293–323 (1.4085–1.5640 μm); endmembers 1,2,4, and 8.

Case 2: Bands 221–251 (1.0485–1.1985 μm); endmembers 1,2,3, and 6.

Case 3: Bands 33–63 (0.4653–0.5313 μm); endmembers 1,2,5, and 6.

For the Case 1, the average correlation (between all four endmembers) found is 0.1966 and the average absolute correlation is 0.4741. The lowest and highest singular values are 8.077 and 0.0496, respectively yielding a condition number of 163.0085. For the second case (Case 2), the average correlation is 0.4710 and the average absolute correlation is 0.4735 with a very high correlation between the 2nd and 3rd endmembers of 0.9283. The corresponding lowest and highest singular values now become 7.4132 and 0.0060 with a condition number of 1.2395e + 03. The multicollinear

Table 1
Unmixing results for the three numerical Cases.

	Determinant endmember matrix	Determinant inverse matrix	Average absolute correlation	RMS (e.g., Eq. (2))	Sum of fractions[a]	Highest fraction[a]	Lowest fraction[a]
Case 1	8.1×10^{10}	1.2×10^{-11}	0.466	1.14×10^{-14}	5.52	5.9	−0.47
Case 2	-1.83×10^{8}	-5.48×10^{-9}	0.456	7.6×10^{-12}	−80.61	212	−91
Case 3	2.3×10^{-11}	8.1×10^{12}	0.997	28.45	0.00001	3.8×10^{17}	-7.7×10^{17}

[a] 1 = 100%.

Table 2
SSE of unmixed fractions compared with the true fractions.

	No noise	With noise level 1 (band 1*0.95)	With noise level 2 (band 1*0.9)
Case 1	0	0.0015	0.0122
Case 2	0	133.4830	1122.5938
Case 3	7.1892	6.9315	6.6815

Table 3
SSE of unmixed fractions compared with the true fractions with noise added for four endmembers and 31 spectral bands (see text for discussion).

	No noise	With noise level 1 (band 1*0.95)	With noise level 2 (band 1*0.90)
Case 1	0	0.01956026	0.07823494
Case 2	0	4.49653015	17.98661017
Case 3	0	4.7050061	18.8207139

case (Case 3) shows, as expected serious instability effects in the matrix inversion. The average correlation and average absolute correlation between all four endmembers both being 0.9978 yields a highest and lowest singular value of 6.0685 and 0.0027, respectively and a condition number of 2.2326e + 03.

Similarly to the case with 6 endmembers and 6 bands reported earlier, a mixed spectrum is generated for each case with equal fractions (1/4) for each of the four endmembers and noise is added. Noise is added to band 1 at 5% and 10% levels, respectively. The unmixing results and SSE statistics are recorded and presented in Table 3 showing similarly to the 6 band/6 endmember case the adherent effect of noise in combination with collinearity on the retrieval of fractional abundances, in this case demonstrated for a multidimensional example with 4 endmembers and 31 spectral bands.

2.6. An example from HyMAP hyperspectral image data

So far, our examples dealt with non-spatial data sets: synthetic data and reflectance spectra. A more realistic case is built using an airborne hyperspectral data set. The imaged area is located in the Cabo de Gata national Parc (SE Spain), an area consisting of calc-alkaline volcanic rocks that have undergone extensive hydrothermal resulting in the new formation of minerals such as alunite, kaolinite, illite (for more details see (Van der Meer, 2006a)). Locally these minerals are overlain by a limestone cap. The image data set used is a (375 samples – 285 lines) subset of a HyMAP scene acquired in July 2003 (see also (Van der Meer, 2006a)). The Hyperspectral Mapper (HyMAP) collects 126 bands in the VNIR–SWIR region with small gaps in the 1.4 and 1.9 μm atmospheric water bands. Spatially the instrument has an IFOV of 2.5 mrad along track and 2.0 mrad across track resulting in a pixel size in the order of 3–5 m. The data was atmospherically and geometrically corrected using the ATCOR 4 model.

Based on geologic knowledge and field work four image endmembers were selected: limestone, alunite, kaolinite and illite. Similar to the previous examples, three cases (Case 1: low correlation between endmembers, Case 2: high correlation between two endmembers, and Case 3: high correlation between all endmembers) were generated by spectral subsetting the image data:

Case 1: 15 band subset, bands 104–118, 2.1185–2.3565 μm.

Case 2: 30 band subset, HyMAP bands 97–126, 1.9906–2.4819 μm.

Case 3: All 126 bands, HyMAP bands 1–126, 0.442–2.4819 μm.

The average absolute correlation between the four endmembers for Case 1, 2 and 3, is 0.54, 0.86 and 0.91, respectively. The results of a linear unconstrained unmixing of the HyMAP image with the four endmembers for the 3 Cases is shown in Fig. 1 and the statistics in Table 4. It is evident that the RMS error increases from Case 1 to Case 3, the negative fractions are highest in Case 3 but also relatively high in the other cases (in particular in Case 1). This was unexpected, however can be explained by the relative high correlation between the endmember illite and the other endmembers for the Case 1 (0.78 with limestone and 0.90 with kaolinite). Dropping the illite endmember and running the unmixing with 3 endmembers and the same scenarios as above dramatically reduces the average absolute correlation for the Case 1 (cf. Case 1 = 0.4, Case 2 = 0.81, Case 3 = 0.89), which does not reduce the overall RMS error significantly but it has a strong effect on the negative fractions which is largely reduced (Fig. 2 and Table 5).

3. How to measure collinearity?

We can attempt to provide an objective measure collinearity in two ways: (1) by deriving a measure from the endmember matrix or the inverse matrix based on their singular values or (2) by deriving a measure from the correlation of the endmember spectra.

3.1. Singular values

For (1) we go back to the numerical example and do a singular value decomposition (SVD) of the endmember and inverse matrices to derive the singular (nonnegative, real) values (i.e., the square root of the eigenvalues). The SVD of $\boldsymbol{M}$ is $\boldsymbol{M} = \boldsymbol{U} \sum \boldsymbol{V}^T$ where $\boldsymbol{U}$ and $\boldsymbol{V}$ are both square, unitary and orthogonal matrices and $\sum$ is a diagonal matrix with the singular values of $\boldsymbol{M}$. The implications of these can be best illustrated with a numerical example. Take the endmember

Table 4
Results of linear unconstrained spectral unmixing of the HyMAP subset with 4 endmembers. For each case and for each endmember the values indicate the number of pixels (of a total of 106,875) with fractions <0 (bold) and >1 (italic). The minimum/maximum RMS error is given.

	Limestone	Alunite	Kaolinite	Illite	RMS
Case 3	**33,532**	**79,338**	**39,698**	**627**	28.88
	12	*112*	*270*	*7369*	1031.47
Case 2	**1761**	**18,599**	**59,247**	**27,049**	12.98
	10	*129*	*14*	*495*	326.42
Case 1	**798**	**11,724**	**65,090**	**51,726**	5.74
	13	*127*	*124*	*534*	157.05

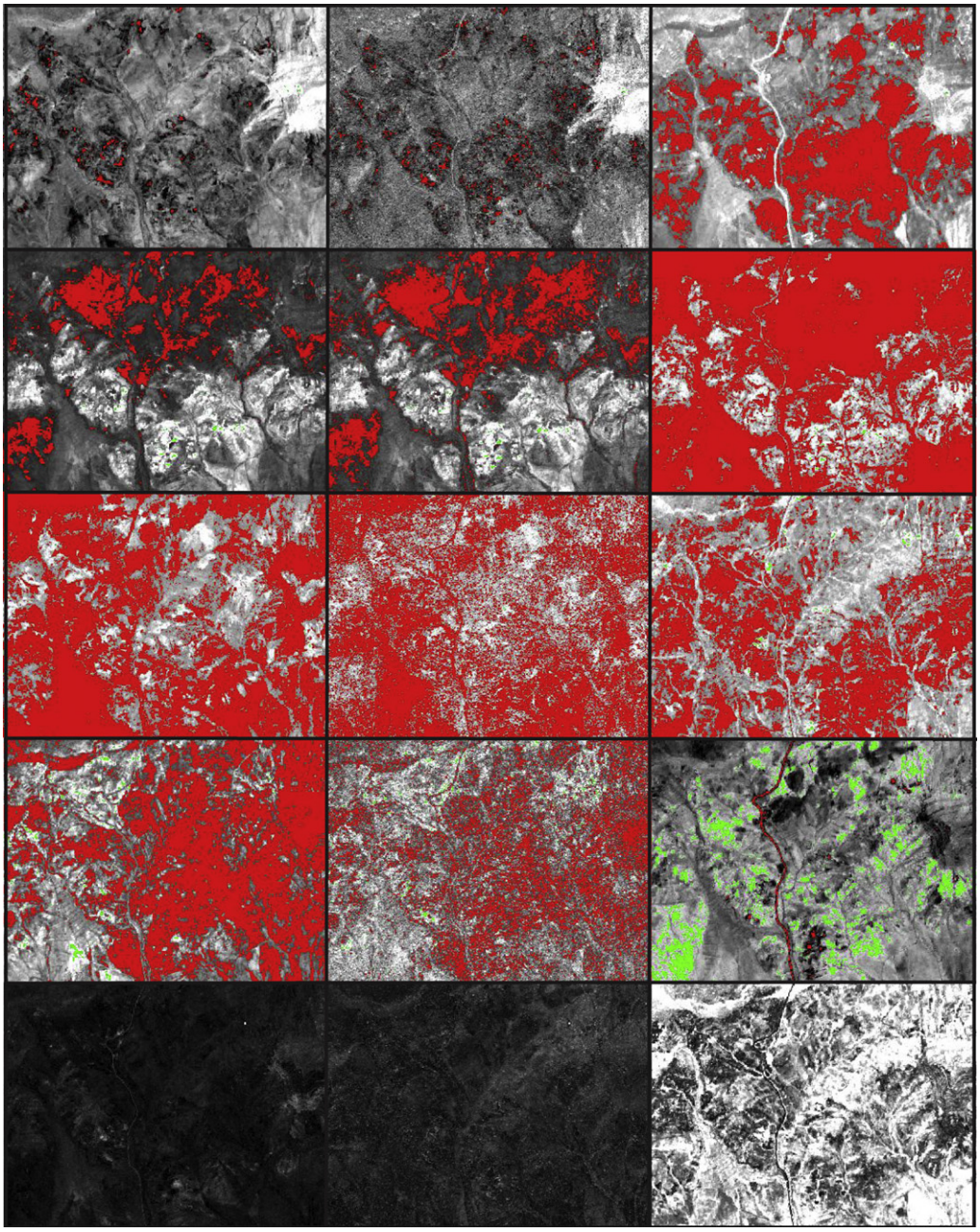

Fig. 1. Unconstrained linear unmixing of a four endmember case. Left to right column Cases 1, 2, 3, respectively. Top to bottom images: limestone fraction, alunite fraction, kaolinite fraction, illite fraction, RMS (all RMS images linearly stretched between 0 and 300). On the fraction images: red, fraction <0; green, fraction >1. (For interpretation of the references to color in this figure legend, the reader is referred to the web version of this article.)

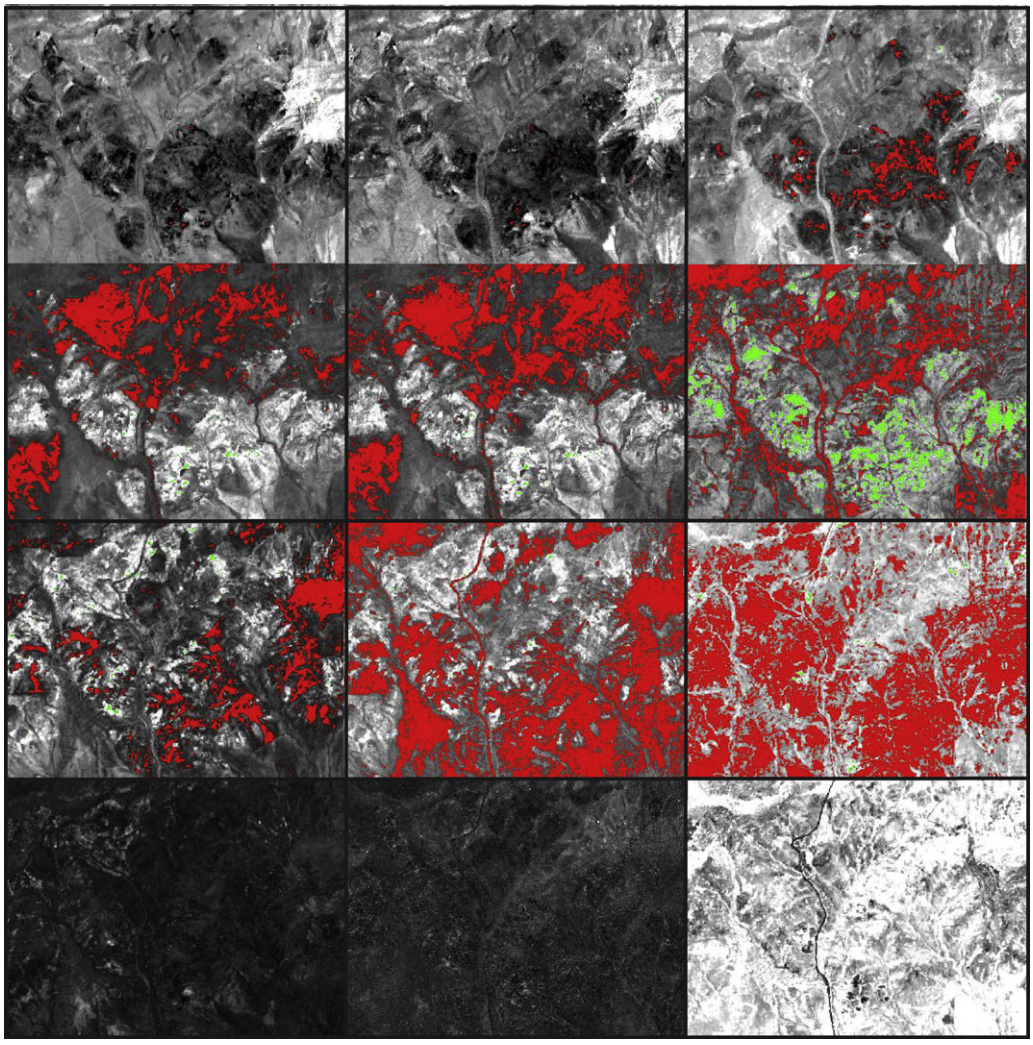

Fig. 2. Unconstrained linear unmixing of a three endmember case. Left to right column Cases 1, 2, 3, respectively. Top to bottom images: limestone fraction, alunite fraction, kaolinite fraction, RMS (all RMS images linearly stretched between 0 and 300). On the fraction images: red, fraction <0; green, fraction >1. (For interpretation of the references to color in this figure legend, the reader is referred to the web version of this article.)

spectra of Eq. (5). The singular value decomposition for this matrix results in

$$\boldsymbol{U} = \begin{bmatrix} -0.2805 & 0.4722 & 0.5379 & 0.1678 & -0.6172 & 0.0036 \\ -0.4054 & 0.3806 & -0.0208 & 0.0281 & 0.4609 & -0.6908 \\ -0.3814 & 0.3660 & -0.3489 & -0.6684 & -0.0302 & 0.3887 \\ -0.5104 & -0.6949 & 0.2364 & -0.3371 & -0.1866 & -0.2286 \\ -0.4451 & -0.1093 & -0.6242 & 0.5686 & -0.2703 & 0.0626 \\ -0.3909 & -0.0589 & 0.3782 & 0.2954 & 0.5458 & 0.5617 \end{bmatrix} \quad (15)$$

$$\boldsymbol{V} = \begin{bmatrix} -0.3489 & -0.1869 & -0.3537 & -0.7404 & 0.4124 & 0.0009 \\ -0.7461 & 0.5415 & 0.2903 & -0.0526 & -0.2312 & -0.0979 \\ -0.0809 & 0.0466 & 0.0396 & 0.0069 & -0.0032 & 0.9948 \\ -0.3341 & -0.7883 & 0.2477 & -0.0145 & -0.4533 & -0.0014 \\ -0.3947 & -0.2177 & 0.0179 & 0.6001 & 0.6603 & -0.0247 \\ -0.2184 & 0.0305 & -0.8529 & 0.2978 & -0.3676 & 0.0115 \end{bmatrix} \quad (16)$$

$$\sum = \begin{bmatrix} 728.52 & 0 & 0 & 0 & 0 & 0 \\ 0 & 175.54 & 0 & 0 & 0 & 0 \\ 0 & 0 & 112.78 & 0 & 0 & 0 \\ 0 & 0 & 0 & 84.47 & 0 & 0 \\ 0 & 0 & 0 & 0 & 54.49 & 0 \\ 0 & 0 & 0 & 0 & 0 & 1.22 \end{bmatrix} \quad (17)$$

The ratio of the highest and the lowest singular value (also known as the matrix condition number) is 728.52/1.22 = 597.15. However the SVD for Eq. (11) yields

$$\sum = \begin{bmatrix} 474.57 & 0 & 0 & 0 & 0 & 0 \\ 0 & 30.48 & 0 & 0 & 0 & 0 \\ 0 & 0 & 11.43 & 0 & 0 & 0 \\ 0 & 0 & 0 & 5.84 & 0 & 0 \\ 0 & 0 & 0 & 0 & 0.73 & 0 \\ 0 & 0 & 0 & 0 & 0 & 2.12 \times 10^{-15} \end{bmatrix} \quad (18)$$

And thus the ratio for the highest and lowest singular value (condition number) is $474.57/2.12 \times 10^{-15} = 2.23 \times 10^{17}$. From the singular values portrayed in Table 6 one can conclude that the higher the condition number the more singular the matrix or a high ratio indicates the presence of collinearity among endmembers. This is particularly reflected in the singular value ratios of the inverse matrices. In general, values of the condition number near 1 indicate a well-conditioned matrix, whereas high values indicate an ill-conditioned matrix. In Fig. 3 condition numbers for increasing correlation between the two endmembers are shown. In the present case the condition number increases exponentially when the correlation exceeds 0.6 indicating that for these levels of

Table 5
Results of linear unconstrained spectral unmixing of the HyMAP subset with 3 endmembers. For each case and for each endmember the values indicate the number of pixels (of a total of 106,875) with fractions <0 (bold) and >1 (italic). The minimum/maximum RMS error is given.

	Limestone	Alunite	Kaolinite	RMS
Case 3	**3204**	**19,227**	**45,772**	30.85
	11	4769	241	1033.75
Case 2	**63**	**20,199**	**37,835**	14.36
	5	116	45	334.92
Case 1	**50**	**13,182**	**9202**	6.4
	4	128	214	205.78

correlation the inversion through a linear spectral unmixing becomes prone to errors.

3.2. Endmember correlation

Collinearity and multicollinearity can be demonstrated through the matrix condition number which we have shown is a reliable indicator of collinearity. Yet severity/impact is not related in an obvious way to the condition number thus the cause and effects are difficult to predict because the effect on the response can be (1) due to single endmember spectrum (one-on-one) that is highly correlated (as in the case of 2), (2) due to multiple collinearity issues (i.e., pairs of endmembers are highly correlated, as Case 3), (3) due to true multi-collinearity where several explanatory variables (endmembers) are correlated, (4) due to spectral response functions (e.g., bands within a spectrum) that contain overlapping and thus redundant information and (5) may also result from multiple scattering of photons with various materials within a pixel.

Table 7 shows a correlation matrix of typical alteration (clay, feldspar, sulfate) minerals used in geologic studies, whereas Table 8 shows the same sets of mineral but now using the shortwave infrared (SWIR) part of the spectrum where these minerals exhibit their diagnostic absorption areas. Indicated in bold in these tables are the highly correlated endmembers. It is evident from the comparison of Tables 7 and 8 that by zooming in on the spectral range where the minerals exhibit diagnostic absorption features dramatically increases the pairwise correlation. Recall Fig. 3, it is evident that in many cases (even more pronounced in the SWIR bands) the level of correlation exceeds 0.6, which poses problems in the matrix inversion during an unmixing analysis. By using only the SWIR bands, which is logical from a mineralogical perspective as this is the spectral range where the minerals exhibit diagnostic absorption features, the pairwise correlation increases and many mineral pairs now exhibit correlation coefficients above the 0.6 which we identified earlier (cf. Fig. 3) to be a critical level.

In Fig. 4, a comparison is shown of the correlation versus spectral resolution (original is ± 1 nm spectral sampling and ±1 nm spectral resolution) for a spectrum of the mineral kaolinite using the 0.4–2.5 μm range and the 2.0–2.5 μm where the original spectrum is degraded to coarser spectral resolution and the correlation with the original high resolution spectrum is calculated. When exceeding a resolution of approximately 12–15 nm (which is the order

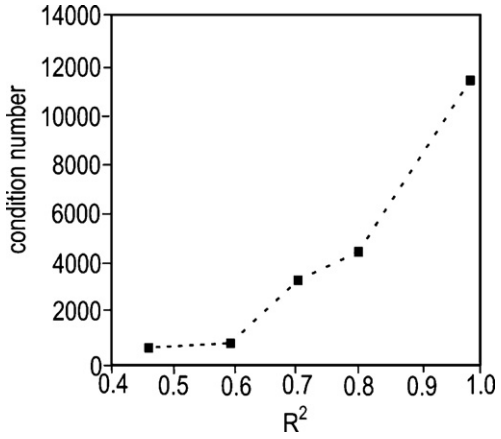

Fig. 3. Condition number for $(\boldsymbol{M}^T\boldsymbol{M})^{-1}$ versus the correlation between two endmembers for a collinear case showing the matrix becomes ill-defined with a level of correlation exceeding 0.6.

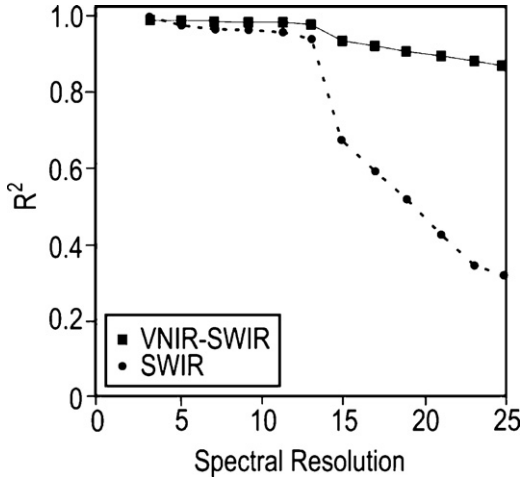

Fig. 4. Correlation (between the original and the degraded spectrum) versus spectral resolution (original is ±1 nm spectral sampling and ±1 nm spectral resolution) for a spectrum of the mineral kaolinite using the 0.4–2.5 μm range and the 2.0–2.5 μm (which contains the diagnostic absorption features).

of magnitude of the width of the diagnostic mineral absorption features) we start to see the effect of resolution on the correlation.

The above effect of the spectral sampling/resolution in relation to the width of the diagnostic absorption features on the response also depends on the correlation of the mixed pixel spectrum against the endmember spectra. In statistics, spurious correlations among variables are common as in endmember statistics. In spectrally unmixing of large scenes specific endmembers may be overlooked which will be expressed in negative or large positive fractions which are typical 'statistical artifacts' of forcing an unmixing solution. In addition, an endmember spectrum often is a mixture of two other spectra or a combination of target spectral response and adjacency effects (i.e., scattered radiation areas surrounding the target

Table 6
Results of singular values for the three numerical cases.

	Case 1		Case 2		Case 3	
	Endmember matrix	Inverse matrix	Endmember matrix	Inverse matrix	Endmember matrix	Inverse matrix
Highest SV	728.52	0.81	689.19	16.08	474.57	4.5×10^{16}
Lowest SV[a]	1.22	0.0020	0.062	0.0014	2.12×10^{-15}	0.0048
Condition number[b]	597.15	405.0	11,080.22	11,485.71	2.23×10^{17}	9.38×10^{18}

[a] SV = singular value.
[b] Highest SV/lowest SV.

Table 7
Correlation matrix for reflectance spectra of common alteration minerals (±1 nm sampling interval, ±1 nm spectral resolution) for the full 0.4–2.5 μm range.

	Alunite	Buddingtonite	Chlorite	Halloysite	Illite	Kaolinite	Montmorillonite	Talc
Alunite	1.00							
Budddingtonite	0.22	1.00						
Chlorite	−0.52	0.40	1.00					
Halloysite	**0.87**	0.01	**−0.66**	1.00				
Illite	−0.51	0.17	**0.84**	−0.58	1.00			
Kaolinite	**0.88**	0.31	−0.34	**0.90**	−0.33	1.00		
Montmorillonite	**0.67**	**0.67**	−0.08	**0.66**	−0.14	**0.80**	1.00	
Talc	0.59	0.19	0.03	0.59	−0.02	**0.75**	0.56	1.00

Table 8
Correlation matrix for reflectance spectra of common alteration minerals (±1 nm sampling interval, ±1 nm spectral resolution) for the full 2.0–2.5 μm range.

	Alunite	Buddingtonite	Chlorite	Halloysite	Illite	Kaolinite	Montmorillonite	Talc
Alunite	1.00							
Budddingtonite	−0.13	1.00						
Chlorite	0.14	**−0.94**	1.00					
Halloysite	**0.73**	**−0.66**	**0.67**	1.00				
Illite	0.51	**−0.82**	**0.81**	**0.92**	1.00			
Kaolinite	**0.75**	**−0.63**	**0.65**	**0.99**	**0.89**	1.00		
Montmorillonite	0.57	**−0.81**	**0.75**	**0.88**	**0.94**	**0.84**	1.00	
Talc	0.11	**−0.86**	**0.93**	0.58	**0.66**	0.59	**0.61**	1.00

Table 9
Example of modified probability of spectral discrimination with an arbitrary set of three endmembers with multiple correlation coefficients.

	Em1	Em2	Em3
Em1	1		
Em2	0.6	1	
Em3	0.2	0.3	1

area). Adjacency effects can be confounding factors contributing to multicollinearity. Spurious correlation could be due to noise or, in some cases, a non-observed covariate with a strong correlation to one or more endmembers. From the correlation matrix an average correlation that includes multicollinearity (Van der Meer and De Jong, 2000a) can be derived by weighing against the absolute fractions of the endmember sets as

$$\hat{p} = \rho_{ij}\left(\frac{f_{ij}}{f_{ij}+f_{ik}+f_{jk},\ldots,f_{nm}}\right) + \rho_{ik}\left(\frac{f_{ik}}{f_{ij}+f_{ik}+f_{jk},\ldots,f_{nm}}\right) + \rho_{jk}\left(\frac{f_{jk}}{f_{ij}+f_{ik}+f_{jk},\ldots,f_{nm}}\right),\ldots, \rho_{nm}\left(\frac{f_{nm}}{f_{ij}+f_{ik}+f_{jk},\ldots,f_{nm}}\right) \quad (19)$$

An alternative collinearity measure that can be derived from the endmember correlation matrix is the modified measure of spectral discrimination (Van der Meer, 2006b) which for a pixel $\boldsymbol{t}$ and a set of endmember spectra s_k can be derived as

$$\rho_{t,s}(k) = \frac{m(\boldsymbol{t}, s_k)}{\sum_{j=1}^{L} m(\boldsymbol{t}, s_j)}, \quad \text{for } k = 1,\ldots,K \quad (20)$$

where $m(\boldsymbol{t}, s_k)$ is the sum of all correlations for the target spectrum, t, relative to the other spectra in the spectral library (or endmembers) s_k. The denominator of Eq. (20) is the sum of the correlation coefficients of the endmember spectra pairwise against the mixed pixel spectrum. For example this could becomes $\sum_{j=1}^{L} m(\boldsymbol{t}, S_j) = 0.3 + 0.25 + 0.25 + 0.35 = 0.9$. Given the correlation coefficients of the endmembers of Table 9 the modified measure would be $\rho_{t,s}(k=3) = (0.6/0.9) + (0.2/0.9) + (0.3/0.9) = 1$, 22. Thus if the multiple correlation between the endmembers is higher than the pairwise correlation of the endmembers and the mixture the index would be >1 else it is <1.

A common measure of collinearity in statistics is the variance inflation factor (VIF). For Eq. (1), $r_i = \sum_{j=1}^{n} f_j r_{ji} + \varepsilon_i$, the variance of the estimate given the standard deviation, σ, of the error term is

$$var(\hat{f}_j) = \frac{\sigma^2}{(n-1)var(r_j)} x \frac{1}{1-R_j^2} \quad (21)$$

The second term is the VIF where R_j^2 is the coefficient of determination (i.e., one minus the residual sum of squares divided by total sum of squares) which formally is the ratio of the explained variation to the total variation (invariant to the scaling of parameters), however in endmember statistics this is the dependent variable regressed on all endmember vectors. The VIF is 1 for an orthogonal matrix in which all endmembers are uncorrelated. The square root of the VIF can be interpreted as the magnification of the standard error compared to the uncorrelated case so a VIF of 4 means the error is 2 times as large as in the case of independent variables. Typically a rule of thumb is that a VIF > 10 causes serious problems in the inversion and requires collinearity to be dealt with although a recent study (O'Brien, 2007) biases these conclusions and suggest to examine this case by case. An alternative statistic is the partial regression coefficient in case the data are standardized to a mean of zero and unit variance is (Fox and Monette, 1992).

$$\rho = \frac{r_{y1} - r_{y2}r_{12}}{1 - r_{12}^2} \quad (22)$$

where r_{y1} is the correlation between the response and the predictor, r_{y2} is the correlation between the response and the confounder, r_{12} and its square are the correlation and coefficient of determination between predictor and confounder. In the absence of multicollinearity the terms r_{12} and r_{12}^2 are zero and $\rho = r_{y1}$. Thus the deviation of ρ from r_{y1} is a measure of collinearity. Note that the partial correlation can only 'spot' collinearity, not multiple collinearity (which can be serious but go undetected with this partial correlation coefficient).

To illustrate these measures a number of simulations were performed on pure mineral spectra from a spectral library. The theoretical VIF in relation to the R^2 is shown in Fig. 5a. Fig. 5b shows the effect of the spatial weighing of the R^2 using Eq. (11) on the VIF for highly correlated fractions ranging from 100% spatially correlated to 20% spatially correlated. In Fig. 5c the effect of including

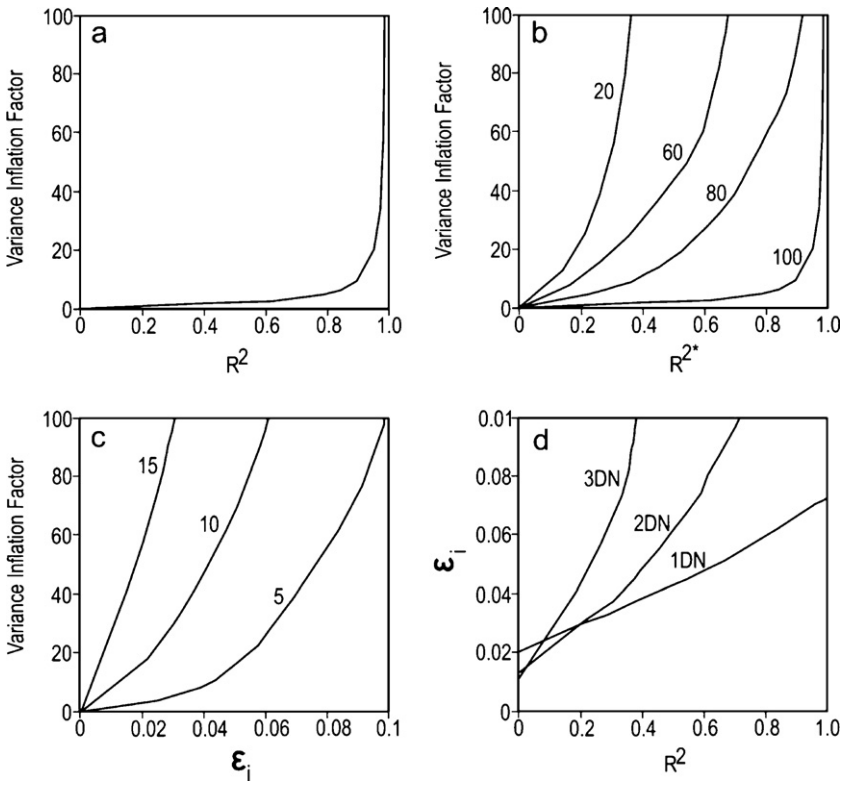

Fig. 5. (a) Theoretical relationship between variance inflation factor (VIF) and R^2, (b) R^2 adjusted for the fractional cover of the correlation of endmembers (based on Eq. (11)) as a function of VIF for fractions ranging from 20 to 100%, (c) relation of VIF and ε_i for a variable endmember set ranging from 5 to 15 endmembers, and (d) relation between ε_i and R^2 for a set of endmembers with random noise added (DN, digital number).

more endmembers is simulated. The likeliness that endmembers are highly correlated increases with the number of endmembers and this is reflected in the VIF and in the value of error term ε_i which reflects the stability of the inversion process. Fig. 5d shows the effect of adding random noise to the endmember spectra. This reduces the multicollinearity of the endmembers but in the mean time it increases collinearity as the ε_i increases. These two effects are entangled and cannot be separated.

4. How to reduce the effect of collinearity?

4.1. Excluding endmembers

The most common method of dealing with collinearity (other than ignoring the effect) is to remove collinear endmembers. This however poses two problems: (1) when two endmember are highly correlated the question arises which one should be excluded and on the basis of what (statistic), and (2) when a highly correlated endmember is excluded it may contain some useful information which would result in destabilizing the mixture model. Alternatively one could be collapsing endmembers; this means clump similar/highly correlated endmembers together to form one new endmember. This is likely to reduce the pairwise correlation but the drawback is that it will inevitably results in missed classes or similar problems to excluding endmembers.

4.2. Decorrelating endmembers

There are a number of transformations such as the principal component transformation or the minimum (or maximum as Green and co-authors introduced it) noise fraction (MNF) transformation (Green et al., 1988) that could be applied to decorrelate endmembers because these decorrelate the band to band correlation. When applied with the same rotation statistics to the image and endmember set (provided these are sampled with the same band set) this would reduce multicollinearity. However the obvious drawback is that we now end up with endmembers whose spectral response has no physical meaning. One could think of alternative approaches to decorrelate endmembers. The most obvious ones are spatial and spectral subsetting. With high spectral resolution (hyperspectral) data it would be an option to partition the spectral dimension into the visible, near infrared and shortwave infrared part where the visible and near infrared allows to study oxides (in soil and rock) and vegetation and the shortwave infrared allows to study clay and sulfate minerals. For hyperspectral analysis it is worthwhile to zoom in on absorption features (or use derivatives such as absorption band depth images) and avoid including the spectral continuum (albedo) which typically is highly correlated between endmembers. Stepwise approaches may be advocated in which we search for areas in the spectrum where the correlation between variables is minimal. In this context, a common approach in spectroscopy uses the partial least squares (PLS) regression on bands that give the best prediction, by exhibiting the highest correlation, to variables to be predicted. Vice versa the PLS approach can be a means to select ranges with least multiple-correlation for unmixing (Westerhuis et al., 2001). Most researchers include all wavebands in the analysis, however this increases the correlation because of the background reflectance and albedo effects.

4.3. Image stratification

Spatial subsetting may help to counter the collinearity problem if the correlated endmembers are spatially exclusive, i.e., they do not coexist in the same parts of the imaged area. Stratified approaches of sampling from a population can be advantageous, however have not been widely used in the spectral unmixing

literature. Stratification can be considered on pre-existing ancillary data (land use/cover information, transportation networks, census data, etc.) or on higher spatial resolution image data. The latter could be considered to solve collinearity issues that have a clear spatial connotation. A study on land cover classification with spectral unmixing showed that local calibrations produced more accurate fractions than global calibrations through stratification of areas where local endmembers and models are representative (Thof and Fraser, 2007). On the contrary, another study on land cover classification using mulitemporal MODIS images and a comparative analysis of an entire-region approach versus an ecoregion-stratified approach showed that stratification did not significantly improve classification accuracies (Shao and Lunetta, 2011). Stratification is not straightforward nor objective. In an attempt to produce a unbiased stratification, object based techniques (geobia/obia) were applied for image segmentation prior to spectra unmixing within polygons which improved the overall accuracy (Hostert et al., 2005). As the results are inconclusive in term of improvement of mapping accuracies, it can be concluded (Weng and Lu, 2008) that stratification in relation to spectral unmixing is an area to further explore.

4.4. Iterative approaches

A number of algorithms automatically find the extreme pixels in a N(band)-dimensional feature space where these extremes are considered to purest (least correlated) spectral endmembers in the scene (Nascimento and Dias, 2005). The N-FINDR algorithm (Winter, 1999) finds the simplex of maximum volume within a hyperspectral data set. However it was recently shown (Zortea and Plaza, 2009) that the resulting endmember set is dependent on the initialization of the algorithm which introduces a bias which led to alternative algorithms that address the issue of random initial endmembers (Chang et al., 2010a; Wu et al., 2009).

These approaches derive endmembers from image statistics such that the endmember set best explains all spectral variability in the image with the least number of uncorrelated (or correlated) endmembers or finding endmembers that form the vertices of the spectral cloud (i.e., simplex) in the feature space but lie within the feature space (Ifarraguerri and Chang, 1999). These are not only likely to be the purest (homogenous) endmembers but are also likely to be the least cross correlated. One such approach is the convex cone analysis and the pixel purity index (Chang and Plaza, 2006; Chang et al., 2010b). Although likely PPI will return a set of n pure endmembers best characterizing the spectral variation in the scene (where n is dependent on the parameter settings and implementation of the algorithm, thus PPI does not ensure a unique set of endmembers), the endmembers may not necessary represent materials of interest to the user. Imagine a geologist interested in mapping alteration mineralogy. (S)He has a clear concept of key minerals and a model in mind that spatially constrains the sequence of surface mineralogy representing the changes in P–T conditions of the system in relation to fluid chemistry and host rock mineralogy. The key minerals unfortunately all are clay and sulfate minerals that have diagnostic features in the SWIR region and are highly correlated. It is unlikely that these will represent all spectral variability and hence unlikely that a statistical method such as PPI will return these. Nevertheless from a data mining perspective such techniques are interesting to explore.

An interesting alternative are the endmember bundles approach (Bateson et al., 2000). These bundles represent a range of spectra for each endmember which could be used empirically in combinations with bundles of other endmembers to find the lowest error associated with the matrix inversion or by selecting the subset of bundle spectra that show the least cross correlation.

An iterative approach was proposed in which pixel spectra are added to an endmember set to satisfy optimization criteria including minimizing the mean RMS, minimizing the spread of the RMS values and 'minimizing the spatial structure' in the RMS values (Van der Meer, 1999). Assuming the 'missed endmembers' occur locally, this would imply that there are local maxima in the RMS values which appears as spatial patterns in these images. By adding local endmembers the RMS is reduced and the image gets a 'salt and pepper' appearance. In iteration endmembers are added or replaced dependent on whether these criteria are improved. It was proposed to find an optimal per-pixel endmember set from the image using a two step approach where by iterative unconstrained unmixing in each iteration one endmember (based on minimum abundance) is removed after which an analysis of the root-mean-square error is used to derive a fitness function to determine the critical iteration defining the optimal endmember set (Rogge et al., 2006). The drawback of all iterative approaches and techniques that use statistics to derive image endmembers is that these may well lead to an optimal mixture model for the scene but with endmembers that are unlikely to represent targets of interest to the interpreter. Another point of concern with iterative approaches that minimize the RMS is that a low RMS or good fitness does not ensure accurate fraction estimates.

5. Discussion

Collinearity and multicollinearity is inherent in spectral unmixing of image data, however it is largely neglected by the remote sensing community. Most historic papers have focused on the (negative) effect of sensor noise on the inversion process in spectral unmixing. We have shown examples with and without noise added where the inversion is becoming unstable due to collinearity. Using 6×6 matrices we illustrate the problem with a simple matrix inversion using singular value decomposition. Next we add noise to these data sets which accelerates the problem. Using real reflectance spectra we design an experiment with 4 endmembers and 31 bands. Now no longer a synthetic case and a square matrix the inherent problems with collinearity persists when the endmember spectra tend to be non-orthogonal. To get an estimate of the severity of the collinearity problem in an spectral unmixing exercise we propose to either explore the matrix inversion process itself to explore the orthogonality between the endmembers. The singular values and condition number of the matrix are the most direct measure of collinearity the user can get, however most popular software packages hide this from the user. The second best estimate is using the variance inflation factor although we show in a numerical example that the user should be cautious in using the rule of thumb that a VIF > 10 means 'trouble'. The third best thing to do is to explore the multiple correlations between endmembers where we provide a number of metrics (Eqs. (19) and (20)) that allow to arrive at a weighted average endmember correlation. As a rule of thumb, for a correlation >0.6 the user should be starting to become suspicious on the results, however we also have shown (the example in Fig. 1) that one or two very high pairwise correlations that may go unnoticed in the average absolute correlation may serious deteriorate the spectra inversion. There is unfortunately no single recipe to successfully combating collinearity although we propose a number of solutions from the literature. Dropping or excluding endmembers from the analysis will mitigate the problem from a statistical/mathematical perspective, but from a user perspective in many cases this may mean that no surface information is retrieved on what may be an important variable of interest. Similarly trying to find the least correlated (or purest) endmembers using iterative approaches will circumvent the problem from a mathematical perspective, but the endmember set retrieved may not be representing the classes of

interest to the user. Decorrelating endmembers (using PCA or modified PCA approaches such as MNF) will in many cases improve the inversion but the problem is that now also the endmembers are transformed into a space where their response is no longer related to reflectance thus their responses no longer have a physical meaning. Image stratification possibly combined with multiple endmember sets that vary per pixel or image object seems a viable way of dealing with the problem of collinearity in spectral unmixing but there is limited literature on this topic.

Several researchers have attempted to combine spectral information with spatial connectivity to derive at spectrally distinct and uncorrelated endmember sets. The first such methods was based on mathematical morphology (Plaza et al., 2002). Another spatial–spectral endmember extraction technique proposed (Rogge et al., 2007) starts by using singular value decomposition to determine vectors that describe most of the spectral variance for subsets of the image. These are projected onto the full image data to determine a set of candidate endmember which in turn are spatially aggregated to allow separating endmembers that are spectrally similar, but spatially independent. Recently, the concept of spatial purity of pixels as an addition to pixel spectral purity was introduced and spatial neighborhoods were used to integrate spectral and spatial information in endmember selection (Mei et al., 2010). Recently (Martin and Plaza, 2011), a region-based spatial preprocessing approach for endmember extractions was proposed that determines a set of spatially representative regions with associated spectra. Theoretically this approach, although not tested in the paper, could significantly reduce collinearity because it selects out of a predefined set of regions those pixels with associated spectra that are both spectrally pure and orthogonal.

Another metric to further test in terms of its sensitivity to collinearity is a ratio referred to as the InStability Index (Somers et al., 2010) defined as the ratio of the within-class endmember variability and the between-class endmember variability. A value exceeding one indicates the within-class variability exceeds the between-class variability, while the converse is true when ISI drops below one. Simulation studies using least-squares spectral unmixing showed that the accuracy of subpixel fraction estimates linearly decreases with increasing variability within endmember classes and linearly increases with increasing variability among endmembers. This would suggest a potential relation with the underlying inversion algorithm and hence the metric could serve as a measure of collinearity given an empirical or mathematical relationship can be derived.

Near-collinearity or multicollinearity from a mathematical perspective makes the endmember matrix ill-conditioned expressed through the value of its determinant being nearly 0. In regression analysis, Ridge regression is used to fight collinearity issues by modifying the matrix so as to make its determinant different from 0. To do so, a user-defined Ridge parameter is added typically estimated through a cross validation or leave-on-out analysis through which improvements to the inverse model are assessed using an f-statistic. The approach reduces the multiple correlation but also introduces bias to the system. In addition, the cross validation procedure is frequently criticized as by leaving one out the intrinsic statistics of the data set is altered. Likewise a mixture model based on Ridge regression (Shi and Wang, 1999) to fight collinearity could be developed where the near singular matrix $(\boldsymbol{M}^T\boldsymbol{M})^{-1}$ of Eq. (4) can be remodeled $\hat{f} = (\boldsymbol{M}^T\boldsymbol{M} + \boldsymbol{kI})^{-1}\boldsymbol{M}^T\boldsymbol{r}$ where $\boldsymbol{k}$ is the Ridge parameter and $\boldsymbol{I}$ the identity matrix. The Ridge trace, a plot of the regression coefficient as a function of the Ridge parameter, is used to decide on an optimal value of $\boldsymbol{k}$. This concept is similar to regularised covariance estimation where when a class variance is not reliable it is modified by the global data's covariance. As such it also poses similar problems as classical Ridge regression, for example, the bias that is introduced by setting the Ridge parameter.

6. Conclusions

Spectral unmixing techniques strive at calculating the fractional cover of (user) selected endmembers within the volume of a pixel. The mixing problem is a linear system of equations of unknown fractions multiplied by endmember spectra. The solution typically is found through a least squares inversion such as the singular value deconvolution of the endmember matrix. The inversion process is influenced by the orthogonality of the endmembers and thus if endmembers are highly correlated (and collinearity or multi-collinearity occurs) the inversion becomes unstable and the estimated fractions sensitive to random error (e.g., noise). In practice, collinearity almost always exists but it is typically overlooked or ignored. We demonstrated the effect of collinearity on the spectral unmixing. In the presence of noise the inversion model becomes even more unstable. A number of measures have been reviewed to quantify the level of (multi)collinearity in the endmember matrix. Each of these highlights a different influencing factor. From a mathematical perspective the ratio of the highest–lowest singular value expressed in the matrix condition number is the most appropriate. This condition number shows that for the collinear case with a correlation exceeding 0.6 the matrix becomes ill-defined. The weighted multiple correlation measure and the partial regression coefficient emphasize the endmember correlation whereas the variance inflation factor is directly related to the orthogonality of the matrix (VIF = 1 in the orthogonal case and >1 in all other cases). There are several suggested remedies to mitigate the collinearity problem. Most of these focus on the endmember set used in the mixture model. Collinear endmembers can be excluded from the analysis or can be decorrelated. Other researchers have proposed iterative approaches to arrive at a set of endmembers that represent the vertices of the spectral cloud (i.e., simplex) which are the least correlated and most homogenous targets in a scene. Given our analysis, these endmember sets are likely to show the least amount of multicollinearity. We propose to explore an adjustment of the mixing model similar to Ridge regression. In conclusion, collinearity hampers the use of fractional abundance estimates, there is no single recipe to successfully combat this problem but in all mixture models collinearity should be tested.

References

Adams, J.B., Sabol, D.E., Kapos, V., Almeida Filho, R., Roberts, D.A., Smith, M.O., Gillespie, A.R., 1995. Classification of multispectral images based on fractions of endmembers: application to land-cover change in the Brazilian Amazon. Remote Sensing of Environment 52, 137–154.

Adams, J.B., Smith, M.O., Johnson, P.E., 1986. Spectral mixture modeling – a new analysis of rock and soil types at the Viking Lander-1 site. Journal of Geophysical Research 91, 8098–8112.

Adams, J.B., Smith, M.O., Gillespie, A.R., 1993. Imaging spectroscopy: interpretation based on spectral mixture analysis. In: Pieters, C.M., Englert, P. (Eds.), Remote Geochemical Analysis: Elemental and Mineralogical Composition. Cambridge University Press, New York, pp. 145–166.

Asner, G.P., Heidebrecht, K.B., 2002. Spectral unmixing of vegetation, soil and dry carbon cover in arid regions: comparing multispectral and hyperspectral observations. International Journal of Remote Sensing 23, 3939–3958.

Asner, G.P., Lobell, D.B., 2000. A biogeophysical approach for automated SWIR unmixing of soils and vegetation. Remote Sensing of Environment 74, 99–112.

Bateson, C.A., Asner, G.P., Wessman, C.A., 2000. Endmember bundles: a new approach to incorporating endmember variability into spectral mixture analysis. IEEE Transactions on Geoscience and Remote Sensing 38, 1083–1094.

Boardman, J.W., 1989. Inversion of imaging spectrometry data using singular value decomposition. In: Proceedings of Geoscience and Remote Sensing Symposium, IGARSS'89, Vancouver, British Columbia, pp. 2069–2072.

Chang, C.I., 2003. Hyperspectral Imaging: Techniques for Spectral Detection and Classification. Kluwer Academic/Plenum Publishers, New York.

Chang, C.I., Plaza, A., 2006. A fast iterative algorithm for implementation of pixel purity index. IEEE Geoscience and Remote Sensing Letters 3, 63–67.

Chang, C.I., Zhao, X.L., Althouse, M.L.G., Pan, J.J., 1998. Least squares subspace projection approach to mixed pixel classification for hyperspectral images. IEEE Transactions on Geoscience and Remote Sensing 36, 898–912.

Chang, C.I., Wu, C.C., Lo, C.S., Chang, M.L., 2010a. Real-time simplex growing algorithms for hyperspectral endmember extraction. IEEE Transactions on Geoscience and Remote Sensing 48, 1834–1850.
Chang, C.I., Wu, C.C., Chen, H.M., 2010b. Random pixel purity index. IEEE Geoscience and Remote Sensing Letters 7, 324–328.
Chen, J., Jia, X.P., Yang, W., Matsushita, B., 2009. Generalization of subpixel analysis for hyperspectral data with flexibility in spectral similarity measures. IEEE Transactions on Geoscience and Remote Sensing 47, 2165–2171.
Chen, X., Chen, J., Jia, X., WU, J., 2010. Impact of collinearity on linear and nonlinear spectral mixture analysis. In: Benediktsson, J.A. (Ed.), 2nd Workshop on Hyperspectral Image and Signal Processing (WHISPERS): Evolution in remote sensing. IEEE, Reykjavik, Iceland.
Clark, R.N., 1983. Spectral properties of mixtures of montmorillonite and dark carbon grains: implications for remote sensing minerals containing chemically and physically absorbed water. Journal of Geophysical Research 88, 10635–10644.
Cloutis, E.A., 1996. Hyperspectral geological remote sensing: evaluation of analytical techniques. International Journal of Remote Sensing 17, 2215–2242.
de Jong, S.M., Paracchini, M.L., Bertolo, F., Folving, S., Megier, J., de Roo, A.P.J., 1999. Regional assessment of soil erosion using the distributed model SEMMED and remotely sensed data. Catena 37, 291–308.
Drake, N.A., Mackin, S., Settle, J.J., 1999. Mapping vegetation, soils, and geology in semiarid shrublands using spectral matching and mixture modeling of SWIR AVIRIS imagery. Remote Sensing of Environment 68, 12–25.
Foody, G.M., Cox, D.P., 1994. Sub-pixel land-cover composition estimation using linear mixture model and fuzzy membership functions. International Journal of Remote Sensing 15, 619–631.
Fox, J., Monette, G., 1992. Generalized collinearity diagnostics. Journal of the American Statistical Association 87, 178–183.
Graham, M.H., 2003. Confronting multicollinearity in ecological multiple regression. Ecology 84, 2809–2815.
Green, A.A., Berman, M., Switzer, P., Craig, M.D., 1988. A transformation for ordering multispectral data in terms of image quality with implications for noise removal. IEEE Transactions on Geoscience and Remote Sensing 26, 65–74.
Harsanyi, J.C., Chang, C.I., 1994. Hyperspectral image classification and dimensionality reduction – an orthogonal subspace projection approach. IEEE Transactions on Geoscience and Remote Sensing 32, 779–785.
Hecker, C., van der Meijde, M., van der Meer, F.D., 2010. Thermal infrared spectroscopy on feldspars – successes, limitations and their implications for remote sensing. Earth-Science Reviews 103, 60–70.
Hedley, J.D., Mumby, P.J., 2003. A remote sensing method for resolving depth and subpixel composition of aquatic benthos. Limnology and Oceanography 48, 480–488.
Hostert, P., Diermayer, E., Damm, A., Schiefer, S., 2005. Spectral Unmixing Based on Image and Reference Endmembers for Urban Change Analysis. Millpress Science Publishers, Rotterdam.
Hunt, G.R., 1977. Spectral signatures of particulate minerals in the visible and near-infrared. Geophysics 42, 501–513.
Ichoku, C., Karnieli, A., 1996. A review of mixture modeling techniques for sub-pixel land cover estimation. Remote sensing reviews 13, 161–186.
Ifarraguerri, A., Chang, C.I., 1999. Multispectral and hyperspectral image analysis with convex cones. IEEE Transactions on Geoscience and Remote Sensing 37, 756–770.
Johnson, P.E., Smith, M.O., Taylor-George, S., Adams, J.B., 1983. A semiempirical method for analysis of the reflectance spectra of binary mineral mixtures. Journal of Geophysical Research 88, 3557–3561.
Ju, J.C., Kolaczyk, E.D., Gopal, S., 2003. Gaussian mixture discriminant analysis and sub-pixel land cover characterization in remote sensing. Remote Sensing of Environment 84, 550–560.
Keshava, N., Mustard, J.F., 2002. Spectral unmixing. IEEE Signal Processing Magazine 19, 44–57.
Kruse, F.A., Lefkoff, A.B., Dietz, J.B., 1993. Expert system-based mineral mapping in Northern Death-Valley, California Nevada, using the airborne visible infrared imaging spectrometer (AVIRIS). Remote Sensing of Environment 44, 309–336.
Lelong, C.C.D., Pinet, P.C., Poilve, H., 1998. Hyperspectral imaging and stress mapping in agriculture: a case study on wheat in Beauce (France). Remote Sensing of Environment 66, 179–191.
Lu, D., Batistella, M., Moran, E., Mausel, P., 2004. Application of spectral mixture analysis to Amazonian land-use and land-cover classification. International Journal of Remote Sensing 25, 5345–5358.
Martin, G., Plaza, A., 2011. Region-based spatial preprocessing for endmember extraction and spectral unmixing. IEEE Geoscience and Remote Sensing Letters 8, 745–749.
Mei, S.H., He, M.Y., Wang, Z.Y., Feng, D.G., 2010. Spatial purity based endmember extraction for spectral mixture analysis. IEEE Transactions on Geoscience and Remote Sensing 48, 3434–3445.
Metternicht, G.I., Fermont, A., 1998. Estimating erosion surface features by linear mixture modeling. Remote Sensing of Environment 64, 254–265.
Nascimento, J.M.P., Dias, J.M.B., 2005. Vertex component analysis: a fast algorithm to unmix hyperspectral data. IEEE Transactions on Geoscience and Remote Sensing 43, 898–910.
Neville, R.A., Levesque, J., Staenz, K., Nadeau, C., Hauff, P., Borstad, G.A., 2003. Spectral unmixing of hyperspectral imagery for mineral exploration: comparison of results from SFSI and AVIRIS. Canadian Journal of Remote Sensing 29, 99–110.
O'Brien, R.M., 2007. A caution regarding rules of thumb for variance inflation factors. Quality and Quantity 41, 673–690.
Okin, G.S., Roberts, D.A., Murray, B., Okin, W.J., 2001. Practical limits on hyperspectral vegetation discrimination in arid and semiarid environments. Remote Sensing of Environment 77, 212–225.
Plaza, A., Martinez, P., Perez, R., Plaza, J., 2002. Spatial/spectral endmember extraction by multidimensional morphological operations. IEEE Transactions on Geoscience and Remote Sensing 40, 2025–2041.
Price, J.C., 1994. How unique are spectral signatures? Remote Sensing of Environment 49, 181–186.
Roberts, D.A., Smith, M.O., Adams, J.B., 1993. Green vegetation, nonphotosynthetic vegetation, and soils in AVIRIS data. Remote Sensing of Environment 44, 255–269.
Roberts, D.A., Gardner, M., Church, R., Ustin, S., Scheer, G., R.O., G., 1998. Mapping chaparral in the Santa Monica mountains using multiple endmember spectral mixture models. Remote Sensing of Environment, 267–279.
Roessner, S., Segl, K., Heiden, U., Kaufmann, H., 2001. Automated differentiation of urban surfaces based on airborne hyperspectral imagery. IEEE Transactions on Geoscience and Remote Sensing 39, 1525–1532.
Rogge, D.M., Rivard, B., Zhang, J., Feng, J., 2006. Iterative spectral unmixing for optimizing per-pixel endmember sets. IEEE Transactions on Geoscience and Remote Sensing 44, 3725–3736.
Rogge, D.M., Rivard, B., Zhang, J., Sanchez, A., Harris, J., Feng, J., 2007. Integration of spatial–spectral information for the improved extraction of endmembers. Remote Sensing of Environment 110, 287–303.
Sabol, D.E., Adams, J.B., Smith, M.O., 1992. Quantitative subpixel spectral detection of targets in multispectral images. Journal of Geophysical Research 97, 2659–2672.
Segl, K., Roessner, S., Heiden, U., Kaufmann, H., 2003. Fusion of spectral and shape features for identification of urban surface cover types using reflective and thermal hyperspectral data. ISPRS Journal of Photogrammetry and Remote Sensing 58, 99–112.
Settle, J.J., Drake, N.A., 1993. Linear mixing and the estimation of ground cover proportions. International Journal of Remote Sensing 14, 1159–1177.
Shao, Y., Lunetta, R.S., 2011. Sub-pixel mapping of tree canopy, impervious surfaces, and cropland in the Laurentian Great Lakes Basin using MODIS time-series data. IEEE Journal of Selected Topics in Applied Earth Observations and Remote Sensing 4, 336–347.
Shi, L., Wang, X.R., 1999. Local influence in ridge regression. Computational Statistics and Data Analysis 31, 341–353.
Singer, R.B., 1981. Near-infrared spectral reflectance of mineral mixtures: systematic combinations of pyroxenes, olivine, and iron oxides. Journal of Geophysical Research 86, 7967–7982.
Singer, R.B., McCord, T.B., 1979. Mars: large scale mixing of bright and dark surface materials and implications for analysis of spectral reflectance. In: Proceedings of the 10th Lunar and Planetary Science Conference, Houston, U.S, pp. 1835–1848.
Somers, B., Delalieux, S., Verstraeten, W.W., van Aardt, J.A.N., Albrigo, G.L., Coppin, P., 2010. An automated waveband selection technique for optimized hyperspectral mixture analysis. International Journal of Remote Sensing 31, 5549–5568.
Somers, B., Asner, G.P., Tits, L., Coppin, P., 2011. Endmember variability in spectral mixture analysis: a review. Remote Sensing of Environment 115, 1603–1616.
Thof, I., Fraser, R.H., 2007. Mapping northern land cover fractions using Landsat ETM. Remote Sensing of Environment 107, 496–509.
Tompkins, S., Mustard, J.F., Pieters, C.M., Forsyth, D.W., 1997. Optimization of endmembers for spectral mixture analysis. Remote Sensing of Environment 59, 472–489.
Van der Meer, F., 1999. Iterative spectral unmixing (ISU). International Journal of Remote Sensing 20, 3431–3436.
Van der Meer, F., 2006a. Indicator kriging applied to absorption band analysis in hyperspectral imagery: a case study from the Rodalquilar epithermal gold mining area, SE Spain. International Journal of Applied Earth Observation and Geoinformation 8, 61–72.
Van der Meer, F., 2006b. The effectiveness of spectral similarity measures for the analysis of hyperspectral imagery. International Journal of Applied Earth Observation and Geoinformation 8, 3–17.
Van der Meer, F., De Jong, S.M., 2000a. Improving the results of spectral unmixing of Landsat Thematic Mapper imagery by enhancing the orthogonality of endmembers. International Journal of Remote Sensing 21, 2781–2797.
Van der Meer, F., De Jong, S., 2000b. Imaging Spectrometry: Basic Principles and Prospective Applications. Kluwer academic publishers, Dordrecht.
Vane, G., Green, R.O., Chrien, T.G., Enmark, H.T., Hansen, E.G., Porter, W.M., 1993. The airborne visible infrared imaging spectrometer (AVIRIS). Remote Sensing of Environment 44, 127–143.
Weng, Q.H., Lu, D.S., 2008. A sub-pixel analysis of urbanization effect on land surface temperature and its interplay with impervious surface and vegetation coverage in Indianapolis, United States. International Journal of Applied Earth Observation and Geoinformation 10, 68–83.
Westerhuis, J.A., de Jong, S., Smilde, A.K., 2001. Direct orthogonal signal correction, chemometrics intell. Laboratory Systems 56, 13–25.
Winter, M.E., 1999. N-FINDR: an algorithm for fast autonomous spectral endmember determination in hyperspectral data. In: Descour, M.R., Shen, S.S. (Eds.), Imaging Spectrometry V. Spie-Int Soc Optical Engineering, Bellingham, pp. 266–275.
Wu, C.C., Chang, C.I., Ren, H.S., Chang, Y.L., 2009. IEEE, real-time processing of simplex growing algorithm. In: 2009 IEEE International Geoscience and Remote Sensing Symposium, vol. 1–5. IEEE, New York, pp. 3645–3648.
Zortea, M., Plaza, A., 2009. A quantitative and comparative analysis of different implementations of N-FINDR: a fast endmember extraction algorithm. IEEE Geoscience and Remote Sensing Letters 6, 787–791.